Two Coordination Polymers Based on Pamoic Acid and (1,4-Bis(imidazol-1-yl)-butane: Synthesis, Structures and Properties①

TU Chang-Zheng YANG Yu-Ting WANG Fan
WANG Jian-Ling YIN Hong-Ju CHENG Fei-Xiang②
(*College of Chemistry and Environmental Science, Qujing Normal University, Qujing* 655011, *China*)

ABSTRACT Two mixed-ligand compounds, namely $[Mn_2(bimb)(PA)_2]_n$ (**1**) and $[Zn(bimb)(PA)]_n$ (**2**) (H_2PA = pamoic acid, bimb = 1,4-bis(imidazol-1-yl)-butane) have been synthesized under the same solvothermal conditions. Compound **1** can be described as (4,4) topology based on the 4-connected $[Mn_2(COO)_4]$ paddle-wheel units, which contains both rotaxane- and catenane-like motifs. For **2**, the 2*D* wavy-like network interlocked with each other and resulted in a 2-fold interpenetrated 2*D* → 3*D* architecture. The structural differences of the two compounds are mainly due to the differences of metal ions and coordination modes of the PA^{2-} ligand. In addition, the magnetism and photoluminescent properties of them have also been explored.

Keywords: crystal structures, pamoic acid, luminescence, magnetic properties;
DOI: 10.14102/j.cnki.0254–5861.2011–2946

1 INTRODUCTION

Coordination polymers (Cps) have received more and more attention in recent years due to their structural diversity and promising applications in the areas of catalysis, gas storage, magnetism and optics[1-4]. Particularly, the Cps with magnetism and/or luminescent properties are possibly useful for information storage and emitter for photoluminescence devices[5-7]. The way to generate such Cps is to design ligands and select metal ions ingeniously, and to control the reaction conditions strictly and accurately. It is well known that the structures of such materials are usually governed by the crystallization conditions, including temperature, solvent, template, metal ion, guest, pH value, and so on[8-11]. For example, we have reported two novel Cu(II) Cps by controlling the temperature of the reaction systems recently[12]. Meanwhile, we are also interested in the influence of metal ions on the control of framework topology and the dimensionality of structures.

Pamoic acid (H_2PA) is a very cheap and important feedstock in the chemical industry, which can be used as a counter ion to obtain long-term pharmaceutical preparations of some basic drugs[13, 14]. However, the investigation about this ligand has been far less common in the construction of Cps. To the best of our knowledge, only a few examples have been investigated since the first groups of metal-pamoate coordination complexes were reported in 2007 by Du's group[15-18]. H_2PA is composed of two naphthalene moieties connected with methylene ($-CH_2-$) bridge. The two naphthalene arms can rotate freely around the $-CH_2-$ group by the small change of coordination environments, so as to minimize the steric hindrance and generate unusual structures. We are interested in H_2PA as a bridging ligand, because the molecule can not only build bridges between multiple metal centers, but also show rich coordination modes[19, 20], and the coordination polymers based on such ligand may have unexpected properties.

On the other hand, the employment of mixed ligands has been demonstrated to be an effective approach for constructing diverse Cps. We have obtained many Cps with attractive architectures and properties through the skillful introduction of bis(imidazole) ligands as the coligands in our

Received 27 July 2020; accepted 14 October 2020 (**CCDC 1022408 for 1 and 2012755 for 2**)
① This work was supported by the Shanghai Key Laboratory of Rare Earth Functional Materials, the project of teaching quality and teaching reform of Yunnan Province (2073010023), the National Teaching Quality and Teaching Reform Project (201810684012), the National Natural Science Foundation of China (81601602), and the Innovative Research Team of Functional complexes and Magnetic materials in University of Yunnan Province
② Corresponding author. E-mail: chengfx2019@163.com

previous work[21, 22]. In order to understand the coordination characteristics of H_2PA, we have synthesized the compound $[Mn_2(bimb)(PA)_2]_n$ (**1**), and briefly reported its structure characteristics[23]. Then, under the same synthesis conditions, compound $[Zn(bimb)(PA)]_n$ (**2**) was obtained. For the sake of investigating the influence of metal ions on the framework structures, compounds **1** and **2** were discussed together. The magnetism and photoluminescent properties of them were also studied.

2 EXPERIMENTAL

2. 1 Materials and measurements

All commercially available chemicals were of reagent grade and were used as received without further purification. The ligand 1,4-bis(imidazol-1-yl)-butane (bimb) was synthesized by literature procedures[24, 25]. The infrared spectra were performed on a Varian FT-IR 640 spectrometer with KBr pellets in the 400～4000 cm^{-1} region. Elemental analyses were measured on a Perkin-Elmer 2400 C H N elemental analyzer (C, H and N). Powder X-ray diffraction (PXRD) patterns were collected on a Rigaku D/MAX-IIIC powder diffractometer with Cu-$K\alpha$ radiation. The thermogravimetric analysis (TGA) was performed with a Shimadzu TGA-50H TG analyzer in the range of 25～750 ℃ under a nitrogen flow at a heating rate of 5 ℃/min. The fluorescence excitation and emission spectra were recorded at room temperature with a Hitachi F-4500 spectrophotometer equipped with a 150 W xenon lamp as an excitation source. Magnetic susceptibility measurements were carried out on a Quantum Design MPMSXL SQUID magnetometer and PPMS-9T system. A correction was made for the diamagnetic contribution prior to data analysis.

2. 2 Synthesis of $[Mn_2(bimb)(PA)_2]_n$ (1)

A mixture of $Mn(NO_3)_2·4H_2O$ (0.5 mmol, 0.125 g), H_2PA (0.5 mmol, 0.194 g), bimb (1.0 mmol, 0.190 g), distilled water (1 mL) and C_2H_5OH (5 mL) was placed in a Teflon-lined stainless-steel vessel (23 mL). The mixture was sealed and heated at 160 ℃ for 72 h. After the sample was gradually cooled to room temperature at the rate of 5 ℃/h, brown crystals of **1** were obtained with 69% yield based on Mn. Anal. Calcd. for **1** ($C_{56}H_{38}Mn_2N_4O_{12}$): C, 62.93; H, 3.58; N, 5.24%. Found: C, 62.45; H, 4.26; N, 5.43%. Selected IR data (KBr pellet, cm^{-1}): 3382(m), 2954(s), 2580(s), 1652(s), 1591(s), 1510(vs), 1449(m), 1426(m), 1374(s), 1310(m), 1257(m), 1159(m), 1089(s), 954(s), 840(m), 769(m), 738(m), 662(m).

2. 3 Synthesis of $[Zn(bimb)(PA)]_n$ (2)

The synthesis procedure of compound **2** was similar to that of **1** except that $Mn(NO_3)_2·4H_2O$ was replaced by $Zn(NO_3)_2·6H_2O$. A colorless block-shaped crystal of **2** was obtained with 53% yield based on Zn. Anal. Calcd. for **2** ($C_{33}H_{28}N_4O_6Zn$): C, 61.74; H, 4.40; N, 8.73%. Found: C, 60.98; H, 5.06; N, 8.04%. Selected IR data (KBr pellet, cm^{-1}): 3380(m), 2960(s), 2589(s), 1657(s), 1601(s), 1514(vs), 1452(m), 1426(m), 1377(s), 1315(m), 1257(m), 1152(m), 1074(s), 954(s), 844(m), 763(m), 735(m), 660(m).

We have tried to use chloride, perchlorate, and acetate of Zn(II) and Mn(II) instead of nitrates to prepare compounds **1** and **2**. The results indicating that the anions have no effect on the final products.

2. 4 X-ray crystallography and structure determination

The well-shaped single crystals of **1** and **2** were selected for X-ray diffraction study. The intensity data were collected on a Bruker SMART APEX II CCD diffractometer, operating at 50 kV and 30 mA by using a graphite-monochromated Mo-$K\alpha$ (λ = 0.71073 Å) radiation. Multi-scan absorption corrections were applied with the SADABS program. The structures were solved by direct methods using SHELXS program of the SHELXTL-97 package and refined by full-matrix least-squares fitting on F^2 by SHELXL-97[26, 27]. All non-hydrogen atoms were refined anisotropically, and the hydrogen atoms of organic ligands were located geometrically. Selected bond distances and bond angles are listed in Tables 1 and 2, respectively. Crystal data for **1**: triclinic, space group $P\bar{1}$, a = 9.2324(18), b = 11.197(2), c = 12.943(3) Å, α = 102.60(3)°, β = 99.39(3)°, γ = 112.91(3)°, V = 1156.1(4) $Å^3$, Z = 1, M_r = 1068.78, D_c = 1.535 Mg/m^3, μ = 0.621 mm^{-1}, F(000) = 548, the final R = 0.0491 and wR = 0.1258 for 5225 observed reflections with $I > 2\sigma(I)$ and R = 0.0694 and wR = 0.1414 for all data (R_{int} = 0.0554). The goodness-of-fit indicator (S) is 1.093. Crystal data for **2**: monoclinic, space group $P2_1/c$, a = 13.314(3), b = 13.926(3), c = 16.392(3) Å, β = 103.87(3)°, V = 2950.8(10) $Å^3$, Z = 4, M_r = 641.96, D_c = 1.445 Mg/m^3, μ = 0.885 mm^{-1}, F(000) = 1328, the final R = 0.0758 and wR = 0.1988 for 6640 observed reflections with $I > 2\sigma(I)$ and R = 0.1218 and wR = 0.2314 for all data (R_{int} = 0.0915). The goodness-of-fit indicator (S) is 1.036.

Table 1. Selected Bond Lengths (Å) and Bond Angles (°) for 1

Bond	Dist.	Bond	Dist.	Bond	Dist.
Mn(1)–(1)	2.109(2)	Mn(1)–O(4)#2	2.125(2)	Mn(1)–N(1)	2.134(2)
Mn(1)–O(2)#3	2.145(2)	O(4)–Mn(1)#2	2.125(2)	O(2)–Mn(1)#3	2.145(2)
Mn(1)–O(3)#4	2.160(2)	O(3)–Mn(1)#5	2.160(2)		
Angle	(°)	Angle	(°)	Angle	(°)
O(1)–Mn(1)–O(4)#2	84.09(10)	O(1)–Mn(1) –N(1)	110.10(10)	O(4)#2–Mn(1)–N(1)	104.63(10)
O(1)–Mn(1)–O(2)#3	154.00(9)	O(4)#2–Mn(1)–O(2)#3	88.52(10)	N(1)–Mn(1)–O(2)#3	95.88(9)
O(1)–Mn(1)–O(3)#4	87.72(9)	O(4)#2–Mn(1)–O(3)#4	153.72(10)	N(1)–Mn(1)–O(3)#4	101.63(10)
O(2)#3–Mn(1)–O(3)#4	88.01(9)				

Symmetry transformations used to generate the equivalent atoms: #1: $-x+3, -y+3, -z$; #2: $-x+1, -y+1, -z$; #3: $-x+1, -y+2, -z$; #4: $x, y+1, z$; #5: $x, y-1, z$

Table 2. Selected Bond Lengths (Å) and Bond Angles (°) for 2

Bond	Dist.	Bond	Dist.	Bond	Dist.
O(6)–Zn(1)	2.137(4)	Zn(1)–O(4)#2	2.394(5)	N(1)–Zn(1)#3	2.054(4)
O(4)–Zn(1)#4	2.394(5)	Zn(1)–N(1)#1	2.054(4)	Zn(1)–O(3)#2	2.483(4)
O(3)–Zn(1)#4	2.483(4)	Zn(1)–N(2)	1.738(4)		
Angle	(°)	Angle	(°)	Angle	(°)
N(2)–Zn(1)–N(1)#1	104.51(18)	N(1)#1–Zn(1)–O(6)	88.90(16)	N(2)–Zn(1)–O(6)	128.21(16)
N(2)–Zn(1)–O(4)#2	86.05(18)	N(1)#1–Zn(1)–O(4)#2	133.28(15)	O(6)–Zn(1)–O(4)#2	120.17(14)
N(2)–Zn(1)–O(3)#2	130.3(2)	N(1)#1–Zn(1)–O(3)#2	98.62(16)	O(6)–Zn(1)–O(3)#2	95.09(16)
O(4)#2–Zn(1)–O(3)#2	47.50(14)				

Symmetry transformations used to generate the equivalent atoms: #1: $x-1, y, z$; #2: $x, -y+3/2, z-1/2$; #3: $x+1, y, z$; #4: $x, -y+3/2, z+1/2$

3 RESULTS AND DISCUSSION

3. 1 Structural description

3. 1. 1 $[Mn_2(bimb)(PA)_2]_n$ (1)

Single-crystal X-ray diffraction analysis reveals that compound **1** crystallizes in the triclinic, space group $P\bar{1}$. As shown in Fig. 1, each asymmetric unit of **1** has one Mn(II) ion, one PA^{2-} anion and half a bimb ligand (The other half is generated by the operation of an inversion center). The Mn(II) ion is coordinated by four O atoms from four PA^{2-} anions and one N atom of bimb ligand, resulting in the five-coordinated pyramidal $[MnO_4N]$ geometry. The Mn–O/N bond lengths are between 2.109(2) and 2.160(2) Å, all falling in the normal range. PA^{2-} ligand holds the bi(bidentate) coordinated mode with the OH groups, forming intramolecular hydrogen bonds (O(5)–H(2A) ··O(3) 2.606 Å, O(6)–H(1A) ··O(2) 2.598 Å). The dihedral angle between the two naphthyl rings is 82.3°.

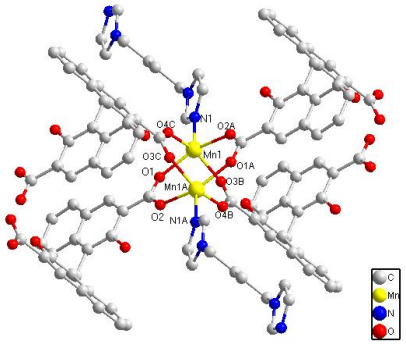

Fig. 1. View of the local coordination environment for Mn(II) centers in 1. Symmetry codes: A: 1 – *x*, 2 – *y*, –*z*; B: *x*, 1 + *y*, *z*

The completely deprotonated PA^{2-} ligand adopts μ_4:η^1,η^1,η^1,η^1 coordination mode (Scheme 1(I)), which acts as two *syn-syn* bridges to connect four Mn(II) ions, resulting in $[Mn_2(COO)_4]$ units. The paddle-wheel $[Mn_2(COO)_4]$ units locating about other inversion centers are linked together by the PA^{2-} ligands, creating the $[Mn_4(PA)_2]$ loop and extended 1*D* tape structure along the *b* direction. Further, the bimb ligand is connected to the tapes via the Mn–N bonds, thus

resulting in the 2*D* net (Fig. 2a). In topology, such a net can be described by (4,4) topology based on the 4-connected $[Mn_2(COO)_4]$ paddle-wheel units. It is worth noting that the fascinating feature of the structure is that it comprises not one but two such nets which interlock with each other in an uncommon way, viz. the $[Mn_4(PA)_2]$ loops of each net are penetrated by one bimb ligand of the other net, and vice versa. Thereby, the structure of **1** cannot be simply considered to consist of two-fold interpenetrating layers, as it has both polyrotaxane and polycatenane characters and is topologically described by the 6-connected net (Fig. 2b). Such feature is consistent with the structure of $Cd_2(L1)(L2)_2$ (L1 = 1,1´-(1,4-butanediyl)bis(imidazole), L2 = pamoic acid) that has been reported by Luo groups[28].

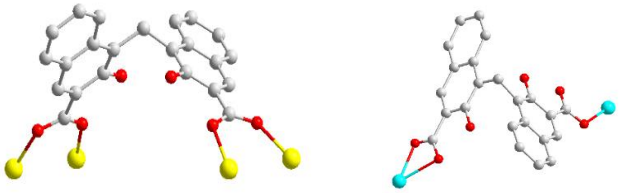

(I) μ_4**:** $\eta^1, \eta^1, \eta^1, \eta^1$ **(II)** μ_2 **:**$\eta^1, \eta^1, \eta^1, \eta^0$

Scheme 1. Coordination modes of PA^{2-} anion

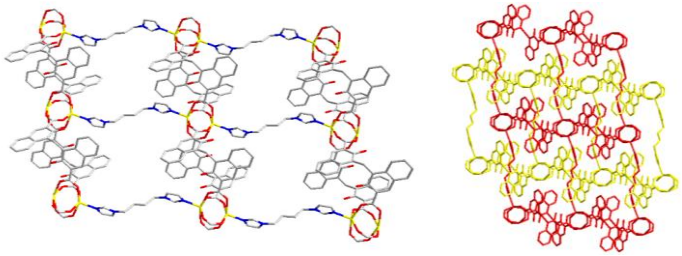

(a) (b)

Fig. 2. (a) 2*D* network of 1. (b) View of the interlocked nets of 1 with its polyrotaxane and polycatenane motifs

3. 1. 2 $[Zn(bimb)(PA)]_n$ (2)

Reactions of the same organic ligands were carried out through the same conditions. Interestingly, the resulting products were largely different for different metal ions. When the metal ion was changed to Zn(II), a 2*D* → 3*D* network $[Zn(bimb)(PA)]_n$ (**2**) formed. Clearly, the kinds of metal ions play a key role in the formation of the final product. As shown in Fig. 3, each Zn(II) ion is five-coordinated and surrounded by two nitrogen atoms of two bimb ligands (Zn(1)–N(2) = 1.738(4) Å, Zn(1)–N(1B) = 2.054(4) Å, B = $x - 1, y, z$) and three carboxyl oxygen atoms of two different PA^{2-} anions (Zn(1)–O(3A) = 2.483(4) Å, Zn(1)–O(4A) = 2.394(5) Å, Zn(1)–O(6) = 2.137(4) Å, A = $x, -y + 1.5, z - 0.5$). Thus, the Zn(II) ion displays a distorted square pyramidal coordination arrangement $[ZnO_3N_2]$. The two carboxyl groups of PA^{2-} ligand adopt monodentate and chelating bidentate bridging coordination modes, respectively (Scheme 1-II) to connect two Zn(II) ions into a zigzag chain. Such chains are further linked by bimb ligand to form a 2*D* wavy-like network (Fig. 4a). The network also can be regarded as undulated (4,4) grid layers, which are arranged in a parallel fashion to afford 1*D* rectangle channels (Fig. 4b).

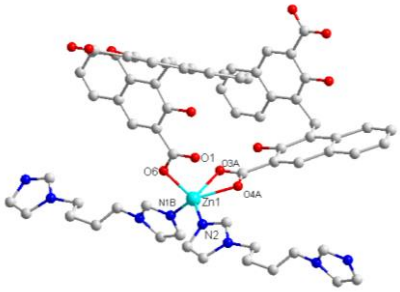

Fig. 3. View of the local coordination environment for Zn(II) centers in 2. Symmetry codes: A = *x*, –*y*+1.5, *z*–0.5; B = *x*–1, *y*, *z*

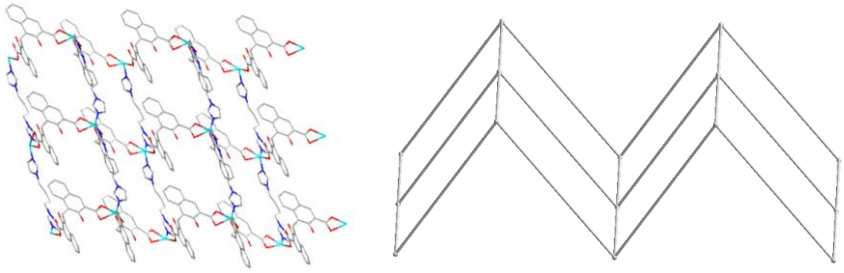

(a) **(b)**

Fig. 4. (a) View of 2*D* network of 2. (b) Schematic description of the 4-connected framework

Both hydroxide groups of PA^{2-} are uncoordinated, and bound to carboxyl O atoms (O(1), O(3)) with strong intramolecular hydrogen bonds of O(5)–H(2A)··O(1) 2.540(3) Å and O(2)–H(1A)··O(3) 2.467(3) Å. The flexible PA^{2-} is twisted and the hydroxy and carboxyl groups adopt a *trans* conformation in order to minimize the steric hindrance. The dihedral angle between both naphthyl rings is 69.8°. Through aborative observation, we found that there are two identical 2*D* undulated networks interlocked with each other, thus directly leading to the formation of a 2-fold interpenetrated 2*D* → 3*D* architecture (Fig. 5a, b).

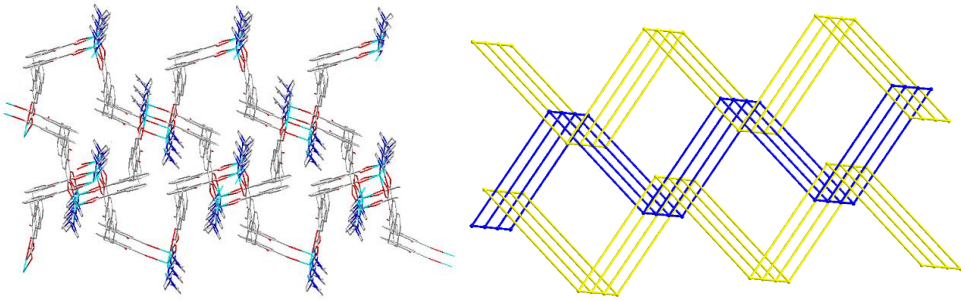

(a) **(b)**

Fig. 5. (a) View of 2*D* → 3*D* network of 2. (b) Schematic representation of the 2-fold interpenetrated structure

3. 3 Thermogravimetric analysis and powder X-ray diffraction

Thermogravimetric analyses (TGA) were carried out to examine the thermal stabilities of synthesized compounds **1** and **2**. The experiments were performed on samples consisting of numerous single crystals of each complex from room temperature to 750 ℃ under the N_2 atmosphere at the heating rate of 5 ℃/min. As shown in Fig. 6, both compounds **1** and **2** display excellent thermal stability. Compound **1** kept intact until about 300 ℃, and then began to decompose upon further heating. For **2**, the rapid weight loss are from about 230 to 481 ℃, which corresponds to the removal of bimb and PA^{2-} ligands. The resulting residue of **2** is ZnO (calcd.: 12.6%, found: 13.2%) after the complete decomposition of the organic ligands.

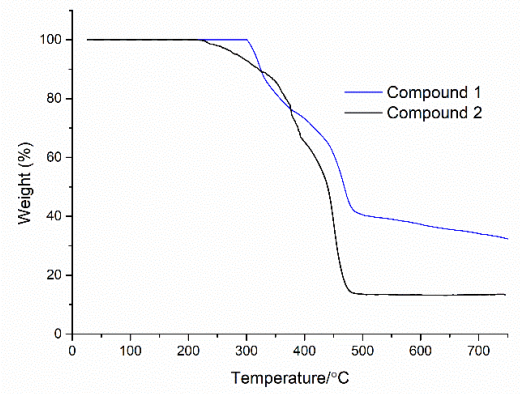

Fig. 6. Thermogravimetric curves of 1 and 2

PXRD was used to check the purity of complexes **1** and **2**. As shown in Fig. 7, all the peaks displayed in the measured patterns for each compound closely match those in the simulated patterns generated from single-crystal diffraction data, indicating that the single phases of **1** and **2** were formed.

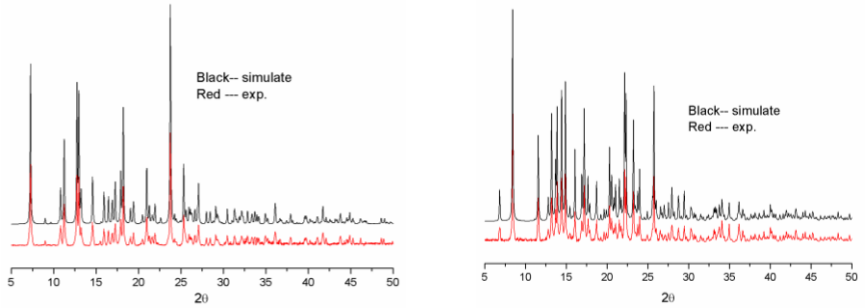

Fig. 7. Exp. and simulated PXRD patterns of 1 and 2

3. 4 Magnetic properties

The magnetic susceptibility measurements for **1** were performed with polycrystalline sample at an applied field of 1000 Oe in the temperature range of 2～300 K. The temperature dependence of $\chi_M T$ and χ_M^{-1} is shown in Fig. 8. At room temperature, the $\chi_M T$ value is 8.40 cm^3 K mol^{-1}, which is comparable with the expected value of 8.75 cm^3 K mol^{-1} (per Mn_2, S = 5/2, g = 2.0[29]). After smooth decrease from 300 to about 84 K, the $\chi_M T$ value decreases sharply and reaches 0.79 cm^3 K mol^{-1} at 2 K. The data above 12 K obeyed the Curie-Weiss law ($\chi = C/(T-\theta)$), resulting in the Curie constant (C) of 9.09 cm^3 K mol^{-1}, and the Weiss constant (θ) of −11.82 K. The Curie constant is in agreement with the expected for two magnetically isolated high-spin Mn(II) ions. The negative values of θ indicate dominating antiferromagnetic coupling between the manganese ions and the shape of the curve is also characteristic of dominant antiferromagnetic exchange interaction, as expected for Mn(II) ions bridged by four *syn-syn* carboxylate groups[30].

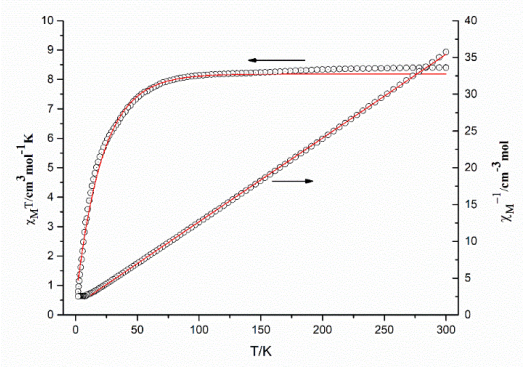

Fig. 8. Plots of the $\chi_M T$ product and χ_M^{-1} versus T for 1. The solid lines represent the best fit to the corresponding classical model and Curie-Weiss law

According to the structure of **1**, two Mn(II) centers are linked by four carboxylate bridges since the coupling through PA^{2-} and bimb ligands can almost be negligible. Thus, two coupling parameters J and zJ' should be considered to interpret the two possible magnetic interactions, in which J is the exchange coupling parameter between Mn1-Mn1A, and zJ' accounts for the rest of interactions. By assuming isotropic exchange, the exchange Hamiltonian of **1** is $H = -2JS_1S_2$, where S = 5/2, and the susceptibility per mol of the paddle wheel dimer unit is given by[30, 31]:

$$\chi'_M = 2\frac{Ng^2\beta^2}{k_BT}\frac{A}{B}$$

$$A = \exp[2J/k_BT] + 5\exp[6J/k_BT] + 14\exp[12J/k_BT] + 30\exp[20J/k_BT] + 55\exp[30J/k_BT]$$

$$B = 1 + 3\exp[2J/k_BT] + 5\exp[6J/k_BT] + 7\exp[12J/k_BT] + 9\exp[20J/k_BT] + 11\exp[30J/k_BT]$$

$$\chi_M = \frac{\chi_M'}{1-(zJ'/Ng^2\beta^2)\chi_M'}$$

where N, g, β, and k_B have their usual meanings. Least-squares analysis of magnetic susceptibility data led to J = –1.36 cm^{-1}, zJ' = –0.22 cm^{-1}, g = 2.03 and R = 1.38 × 10^{-4} (red solid lines in Fig. 8).

3. 4 Photoluminescence properties

Photoluminescent compounds are of great interest currently due to their various applications in chemical sensors, photochemistry, and electroluminescent display. It is well known that metal-organic polymeric complexes with a d^{10} closed-shell electronic configuration have been found to exhibit photoluminescent properties[19]. Here, the photoluminescent property of compound **2** in the solid state at room temperature was examined (Fig. 9). Excitation of the microcrystalline samples at 410 nm leads to the generation of similar fluorescent emissions, with the peak maxima occurring at 552 nm. To further understand the origin of the emission band, the fluorescent spectra of H_2PA and bimb ligands have also been measured. For **2**, the significant red shift of ca. 48 nm relative to that of the free H_2PA ligand shows an emission band at 473 nm (λ_{ex} = 428 nm), and a very obvious red shift of ca. 211 nm relative to that of the free bimb ligand holds an emission band at 341 nm (λ_{ex} = 288 nm). Presumably, the emissions of compound **2** should originate from the intraligand π^*-π transitions[32], whereas the significant redshifts in comparison to H_2PA should be ascribed to the metal-ligand coordinative interactions, and similar red shifts have been observed before[15]. The change of the intensity may result from conformational ligands and weak interactions in the interpenetrating crystalline lattice, which may affect the rigidity of the whole network and further the energy transfer involved in the luminescence[33].

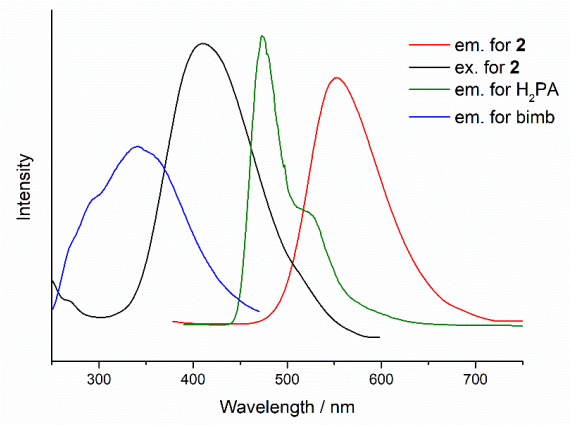

Fig. 9. Emission spectra of 2, H_2PA and bimb in the solid state at room temperature

4 CONCLUSION

In conclusion, in this work we have reported two metal ions-dependent coordination polymers synthesized under the same solvothermal conditions. The PA^{2-} ligand displays different coordination modes in the two compounds. Compound **1** has both polyrotaxane and polycatenane characters. Differently, compound **2** displays a 2-fold interpenetrated 2*D* → 3*D* architecture. Such results reveal that the kinds of metal ions have a great influence on the final structures. Further, magnetic studies show that **1** indicates antiferromagnetic coupling between the adjacent Mn(II) ions, while compound **2** may be good candidate for novel hybrid inorganic-organic photoactive materials.

REFERENCES

(1) Chen, X.; Jiang, H.; Li, X.; Hou, B.; Gong, W.; Wu, X. W.; Han, X.; Zheng, F. F.; Liu, Y.; Jiang, J. W.; Cui, Y. Chiral phosphoric acids in metal-organic frameworks with enhanced acidity and tunable catalytic selectivity. *Angew. Chem. Int. Ed*. **2019**, 58, 14748–14757.

(2) Fan, W. D.; Yuan, S.; Wang, W. J.; Feng, L.; Liu, X. P.; Zhang, X. R.; Wang, X.; Kang, Z. X.; Dai, F. N.; Yuan, D. Q.; Sun, D. F.; Zhou, H. C. Optimizing multivariate metal-organic frameworks for efficient C_2H_2/CO_2 separation. *J. Am. Chem. Soc*. **2020**, 142, 8728–8737.

(3) Cao, C.; Liu, S. J.; Yao, S. L.; Zheng, T. F.; Chen, Y. Q.; Chen, J. L.; Wen, H. R. Spin-canted antiferromagnetic ordering in transition metal-organic frameworks based on tetranuclear clusters with mixed V- and Y-shaped ligands. *Cryst. Growth Des*. **2017**, 17, 4757–4765.

(4) Yao, S. L.; Liu, S. J.; Tian, X. M.; Zheng, T. F.; Cao, C.; Niu, C. Y.; Chen, Y. Q.; Chen, J. L.; Huang, H.; Wen, H. R. A Zn(II)-based metal-organic framework with a rare *tcj* topology as a turn-on fluorescent sensor for acetylacetone. *Inorg. Chem.* **2019**, 58, 3578–3581.

(5) Liu, S. J.; Han, S. D.; Zhao, J. P.; Xu, J.; Bu, X. H. *In-situ* synthesis of molecular magnetorefrigerant materials. *Coord. Chem. Rev.* **2019**, 394, 39–52.

(6) Zhao, Y.; Hao, R. H. Structural diversity and photoluminescent properties of two zinc coordination polymers based on 5-*i*-propoxyisophthalate and flexible N-donor ligands. *Inorg. Nano-Met. Chem*. **2020**, 1–7.

(7) Zhao, Y.; Wang, R. L.; Wu, X. X.; Yang, C. D. A water-stable metal organic framework for the detection of explosives and antibiotics. *Chin. J. Struct. Chem*. **2019**, 38, 991–998.

(8) Li, Z. S.; Li, X. Y.; Liu, J. W.; He, T.; Yue, K. F. Substituent and temperature effect on the assemblies of three lead(II) coordination polymers based on asymmetrical biphenyl tritopic ligands. *Z. Anorg. Allg. Chem.* **2015**, 641, 2570–2575.

(9) Gu, J. Z.; Cui, Y. H.; Liang, X. X.; Wu, J.; Lv, D. Y.; Kirillov, A. M. Structurally distinct metal-organic and H-bonded networks derived from 5-(6-carboxypyridin-3-yl)isophthalic acid: coordination and template effect of 4,4′-bipyridine. *Cryst. Growth Des.* **2016**, 16, 4658–4670.

(10) Dong, X. Y.; Si, C. D.; Fan, Y.; Hu, D. C.; Yao, X. Q.; Yang, Y. X.; Liu, J. C. Effect of N-donor ligands and metal ions on the coordination polymers based on a semirigid carboxylic acid ligand: structures analysis, magnetic properties, and photoluminescence. *Cryst. Growth Des.* **2016**, 16, 2062–2073.

(11) Pinta, N. D.; Fidalgo, L.; Madariaga, G.; Lezama, L.; Cortés, R. Guest driven structural correlations in DPDS [di(4-pyridyl)disulfide]-based coordination polymers. *Cryst. Growth Des.* **2012**, 12, 5069–5078.

(12) Yang, Y. T.; Tu, C. Z.; Miao J. J.; Li J. L.; Chen, G. Temperature-dependent hydrothermal synthesis of two distinct three-dimensional copper complexes. *Chin. J. Struct. Chem.* **2016**, 35, 597–604

(13) Hu, H. Y.; Horton, J. K.; Gryk, M. R.; Prasad, R.; Naron, J. M.; Sun, D. A.; Hecht, S. M.; Wilson. S. H.; Mullen, G. P. Identification of small molecule synthetic inhibitors of DNA polymerase beta by NMR chemical shift mapping. *J. Biol. Chem.* **2004**, 279, 39736–39744.

(14) Jørgensen, M. Quantitative determination of pamoic acid in dog and rat serum by automated ion-pair solid-phase extraction and reversed-phase high-performance liquid chromatography. *Chromatogr. B* **1998**, 716, 315–323.

(15) Du, M.; Li, C. P.; Zhao, X. J.; Yu, Q. Interplay of coordinative and supramolecular interactions in engineering unusual crystalline architectures of low-dimensional metal-pamoate complexes under co-ligand intervention. *CrystEngComm.* **2007**, 9, 1011–1028.

(16) He, Y. P.; Yuan, L. B.; Chen, G. H.; Lin, Q. P.; Wang, F.; Zhang, L.; Zhang, J. Water-soluble and ultrastable Ti_4L_6 tetrahedron with coordination assembly function. *J. Am. Chem. Soc.* **2017**, 139, 16845–16851.

(17) He, Y. P.; Chen, G. H.; Yuan, L. B.; Zhang, L.; Zhang, J. Ti_4(embonate)$_6$ cage-ligand strategy on the construction of metal-organic frameworks with high stability and gas sorption properties. *Inorg. Chem*. **2020**, 59, 964–967.

(18) Chen, G. H.; He, Y. P.; Zhang, S. H.; Zhang, J. Syntheses, crystal structures and fluorescent properties of two metal-organic frameworks based on pamoic acid. *J. Solid State Chem.* **2019**, 270, 335–338.

(19) Shi, X. M.; Li, M. X.; He, X.; Liu, H. J.; Shao, M. Crystal structures and properties of four coordination polymers constructed from flexible pamoic acid. *Polyhedron* **2010**, 29, 2075–2080.

(20) Wang, S. N.; Peng, Y. Q.; Wei, X. L.; Zhang, Q. F.; Wang, D. Q.; Dou, J. M.; Li, D. C.; Bai, J. F. Temperature-dependent supramolecular isomerism in three zinc coordination polymers with pamoic acid and 1,4-bis(imidazol-1-ylmethyl)-benzene. *CrystEngComm.* **2011**, 13, 5313–5316.

(21) Yang, Y. T.; Tu, C. Z.; Yin, H. J.; He, C. X.; Zhao, Q.; Cheng, F. X. Synthesis, structures, and properties of five metal-organic frameworks based on oxidized 3,3′-azodibenzoic acid and different N-donor ligands. *Eur. J. Inorg. Chem.* **2019**, 4582–4591.

(22) Yang, Y. T.; Tu, C. Z.; Xu, L. L.; Yan, B. L.; Wang, F. Flexible bis(benzimidazole)-based ligands directed the structure characteristics of coordination polymers based on diphenic acid Co-ligands: syntheses, structures and properties. *Chin. J. Struct. Chem.* **2019**, 38, 155–164.

(23) Tu, C. Z.; Wang, W. H.; Guo, B.; Miao, J. J.; Yang, Y. T. A novel example of Mn-compound showing rotaxane-like motif. *J. Qujing Normal Univ.* **2014**, 33, 19–22.

(24) Li, S. L.; Lan, Y. Q.; Ma, J. F.; Yang, J.; Wei, G. H.; Zhang, L. P.; Su, Z. M. Structures and luminescent properties of seven coordination polymers of zinc(II) and cadmium(II) with 3,3′,4,4′-benzophenone tetracarboxylate anion and bis(imidazole). *Cryst. Growth Des*. **2008**, 8, 675–684.

(25) Wen, L. L.; Lu, Z. D.; Lin, J. G.; Tian, Z. F.; Zhu, H. Z.; Meng, Q. J. Syntheses, structures, and physical properties of three novel metal-organic frameworks constructed from aromatic polycarboxylate acids and flexible imidazole-based synthons. *Cryst. Growth Des*. **2007**, 7, 93–99.

(26) Sheldrick, G. M. *SHELXS-97, Program for X-ray Crystal Structure Solution*. University of Göttingen, Germany **1997**.

(27) Sheldrick, G. M. *SHELXL-97, Program for the Refinement of Crystal Structures from Diffraction Data*. University of Göttingen, Germany **1997**.

(28) Luo, F.; Yang, Y. T.; Che, Y. X.; Zheng, J. M. An unusual metal-organic framework showing both rotaxane- and cantenane-like motifs. *CrystEngComm*. **2008**, 10, 981–982.

(29) Yi, F. Y.; Sun, Z. M. Solvent-controlled syntheses, structure, and magnetic properties of trinuclear Mn(II)-based metal-organic frameworks. *Cryst. Growth Des*. **2012**, 12, 5693–5700.

(30) Zhao, Y.; Chang, X. H.; Liu, G. Z.; Ma, L. F.; Wang, L. Y. Five Mn(II) coordination polymers based on 2,3′,5,5′-biphenyl tetracarboxylic acid: syntheses, structures, and magnetic properties. *Cryst. Growth Des*. **2015**, 15, 966–974.

(31) Ma, L. F.; Wang, L. Y.; Du, M. A novel 3*D* Mn(II) coordination polymer involving 4,4′-dipyridylsulfide and 4,4′-dipyridyltrisulfide obtained by in situ ligand formation from 4,4′-dipyridyldisulfide. *CrystEngComm*. **2009**, 11, 2593−2596.

(32) Gou, L.; Wu, Q. R.; Hu, H. M.; Qin, T.; Xue, G. L.; Yang, M. L.; Tang, Z. X. An investigation of the positional isomeric effect of terpyridine derivatives: self-assembly of novel cadmium coordination architectures driven by N-donor covalence and $\pi\cdots\pi$ non-covalent interactions. *Polyhedron* **2008**, 27, 1517–1526.

(33) Han, Z. X.; Wang J. J.; Hu, H. M.; Chen, X. L.; Wu, Q. R.; Li, D. S.; Shi, Q. Z. Effects of the size of aromatic chelate ligands and d^{10} metal ions on the structures of dicarboxylate complexes: from dinuclear molecule to helical chains and 2*D* network. *J. Mol. Struct.* **2008**, 891, 364–369.